Am J Transl Res 2020;12(1):1-18
www.ajtr.org /ISSN:2156-6976/AJTR0103656

Original Article

Resveratrol improves high-fat diet-induced insulin resistance in mice by downregulating the lncRNA NONMMUT008655.2

Linyi Shu[1,2], Guangsen Hou[1,2], Hang Zhao[1,2], Wenli Huang[1,2], Guangyao Song[1,2], Huijuan Ma[1,2,3]

[1]Department of Internal Medicine, Hebei Medical University, Shijiazhuang 050017, Hebei, People's Republic of China; [2]Endocrinology Department, Hebei General Hospital, Shijiazhuang 050051, Hebei, People's Republic of China; [3]Hebei Key Laboratory of Metabolic Diseases, Hebei General Hospital, Shijiazhuang 050051, Hebei, People's Republic of China

Received October 17, 2019; Accepted January 3, 2020; Epub January 15, 2020; Published January 30, 2020

Abstract: As essential players in the field of diabetes treatment, resveratrol (RSV) has received much attention in recent years. However, it is unclear whether it can improve insulin resistance by regulating the long-chain non-coding RNA (lncRNA). The objective of this study was to investigate whether RSV improves high-fat diet-induced insulin resistance in mice by regulating thelncRNANONMMUT008655.2 *in vivo* and *in vitro*. To this end, animal and cell insulin resistance models were developed. Specifically, C57BL/6J mice were fed a high-fat diet (HFD) and administered RSV for eight weeks. Additionally, mouse Hepa cells were treated with palmitic acid, transfected with siRNA NONMMUT008655.2, and treated with RSV. Treated mice and cells were then compared to normal controls that were not exposed to RSV. In the animal model, RSV was found to decrease the levels of fasting blood glucose, triglycerides, and low-density lipoprotein cholesterol, as well as the insulin index and area under the curve; while increasing the insulin sensitivity index. Besides, RSV decreased the expression levels of SOCS3, G6PC, and FOXO1 yet increased that of p-Akt and p-FOXO1 in mice. The same results were observed following knockdown of NONMMUT008655.2 in cells. Overall, our results suggest that RSV may improve hepatic insulin resistance and control blood glucose levels by downregulating lncRNA NONMMUT008655.2.

Keywords: Blood glucose, insulin resistance, resveratrol, long-chain non-coding RNA

Introduction

Type-2 diabetes mellitus (T2DM) is one of the leading non-infectious diseases worldwide [1]. Its occurrence is increasing rapidly, with the number of T2DM adults expected to reach 590 million by 2035 [2]. Currently, no specific biomarkers have been identified for T2DM-concurring diseases, and effective treatment options that prevent disease progression are also unavailable. Although a variety of factors lead to T2DM development, insulin resistance (IR) is one of the most significant. IR is a state in which the muscles, fat cells, and liver reduce the uptake and utilisation of glucose [3]. Consequently, the beta cells of the pancreatic islets secrete more insulin to stabilise blood sugar, leading to hyperinsulinemia [4].

Resveratrol (3,4',5-trihydroxy-1,2-stilbene; RSV) is a non-flavonoid polyphenol first isolated in 1940 from the roots of white squash, and subsequently detected in more than 70 plant species, including red grapes, blueberries, mulberries, peanuts, and raspberries [5]. Numerous biological benefits have been reported for RSV, including anti-tumour, antioxidant, anti-inflammatory, cardioprotective, and neuroprotective properties [6]. Several studies have also reported on its anti-IR effects via blood sugar regulation and protection of the islet beta cells [7, 8].

Long non-coding RNA (lncRNA) is a transcription product consisting of more than 200 nucleotides and lacking protein-coding ability. Most lncRNAs are conserved and exhibit lower expression levels than mRNA [9]. Recent studies have shown that lncRNAs are important regulators of numerous biological processes, including proliferation, differentiation, invasion, and apoptosis, while also being associated with insulin resistance-related signalling pathways

and metabolic diseases [10, 11]. However, the role of the lncRNA NONMMUT008655.2 in RSV-mediated improvement of hepatic IR remains unclear. Therefore, the objectives of this study were to investigate the effects of RSV on IR in the mouse liver *in vivo* and *in vitro*, as well as to explore the interrelationship of RSV and NONMMUT008655.2 in improving IR. Cumulatively, our data may provide novel insights into the prevention and treatment of T2DM.

Materials and methods

Animals

Thirty six-week-old, clean grade (body weight, 21.0-23.0 g), male C57BL/6J mice obtained from the Beijing Vital River Laboratory Animal Centre (Licence number: SCXK [Beijing] 2016-0006) were housed in the animal laboratory at the Clinical Research Centre, Hebei Provincial People's Hospital (temperature, 20-25°C; relative humidity, 40-60%; photoperiod, 12 h light/12 h dark) with *ad libitum* access to food and water. The experiment was approved by the Ethics Committee of Hebei General Hospital (approval number: 201920, 19-09-2018) and complies with the International Regulations for the Administration of Laboratory Animals.

Establishment of the animal model

Thirty-six C57BL/6J mice were adaptively fed for one week and then, randomly divided into three groups: 12 in the control (CON) group were fed a regular diet (D12450J; 20% protein, 70% carbohydrates, 10% fat; 3.85 kcal g^{-1}), 12 in the high-fat diet (HFD) group were fed a D1249 diet (20% protein, 20% carbohydrates, 60% fat; 5.24 kcal g^{-1}), and 12 mice in the HFD+RSV group were fed a high-fat diet and administered RSV solution. RSV (Sigma-Aldrich, St. Louis, MO, USA) was dissolved in dimethyl sulfoxide (DMSO; Sigma-Aldrich; 30 mg ml^{-1}) and diluted 1:1 in NaCl 0.9%. The HFD+RSV group was intragastrically administered RSV (100 mg kg^{-1}) daily for six weeks [12], whereas CON and HFD mice were administered NaCl 0.9%, containing 0.1% DMSO.

Weekly body weight and food intake were recorded during mouse breeding. IPGTT was performed after eight weeks of feeding and 12 h of dry fasting. Blood glucose was measured with a blood glucose metre (Johnson & Johnson, New Brunswick, NJ, USA) using blood samples collected from the tail vein at 0 min, 15 min, 30 min, 60 min, and 120 min after a 1.5 g kg^{-1} intraperitoneal injection of 50% glucose diluted 1:1 in NaCl 0.9%. Area under the curve (AUC) was used to validate the establishment of the animal IR model.

Serum and tissue specimens

After six weeks of feeding and 12 h of dry fasting, three randomly selected mice from each group were intraperitoneally administered 37.5 IU kg^{-1} of insulin (Sigma-Aldrich) and euthanised 20 min later by cervical dislocation. Blood was collected by cardiac puncture and centrifuged at 5,000 rpm min^{-1} for 15 min. The upper layer containing serum was transferred into a microcentrifuge tube and stored at -80°C. The liver was quickly dissected and washed with saline solution. A small piece was fixed in 4% paraformaldehyde, whereas the rest of the tissue was placed in a cryotube, frozen in liquid nitrogen, and stored at -80°C.

Determination of blood indicators

Total cholesterol (TC), TG, HDL-C, and LDL-C were determined using kits purchased from the Nanjing Jiancheng Bioengineering Institute (Jiangsu Sheng, China). Serum insulin was determined using an ELISA kit (ALPCO Diagnostics, Salem, NH, USA). All protocols were performed in accordance with manufacturer's instructions.

Haematoxylin-eosin staining

The liver tissue fixed in 4% paraformaldehyde was dehydrated within 24 h of collection with a conventional alcohol gradient (100%, 95%, 80%, 75%). Tissues were then made transparent with xylene, embedded in paraffin, and serially sliced at a thickness of 5 μm. The sections were deparaffinised, treated with haematoxylin for 5 min, differentiated with 70% ethanol for 10 s, and washed with distilled water. After staining with eosin, the sections were dehydrated and sealed with resin. The morphological features of liver sections were observed under a light microscope.

Oil Red O staining

Liver tissue sections were placed in Oil Red O solution for 8-10 min with light protection,

Table 1. Real-time quantitative polymerase chain reaction primers used in this study

Gene	Forward primer (5'-3')	Reverse primer (5'-3')
Actin	GGCGCTTTTGACTCAGGATT	GGGATGTTTGCTCCAACCAA
NONMMUT001470.2	GTGTGGCAGTAATTGAGGCATA	TCCGTCCAGAAGAAAAGACAATA
NONMMUT017329.2	CGGGTTTTTCTCCGTATTCTAA	CACACACACACACAAATGGAAG
NONMMUT047231.2	TTGCAGAGTCGTTTTTCTTATCC	CTCTCAGGAGGAAGAAGCTGAA
NONMMUT031874.2	GCGTGGGACTTATCTTCAGC	ACACACTGCTTCACCACAGG
NONMMUT034345.2	TGGTGAGGAGCAGAAGTGG	TGTGGATGCTATGCTGGAAA
NONMMUT008655.2	TGAGCAAGTTCCACCTGTACC	GTCCCTTCTCTCCTCATTTGC
NONMMUT003114.2	CCTTCACTAGCCCTCCATCA	GTTTCAGGTTCCAGCGACTT
Akt	AAGGAGGTCATCGTCGCCAA	ACAGCCCGAAGTCCGTTATC
FOXO1	AAGGCCATCGAGAGCTCAGC	GATTTTCCGCTCTTGCCTCC
G6PC	TTGCATTCCTGTATGGTAGTGG	TAGGCTGAGGAGGAGAAAACTG
SOCS3	CTGCTTTGTCTCTCCTATGTGG	GAATCCCTCAACTCTCTGCCTA

rinsed with distilled water, differentiated with 75% alcohol, and washed with distilled water. After staining with haematoxylin, the tablets were sealed with glycerine gelatine. The morphological features of liver sections were observed under a light microscope.

Western blot analysis

Proteins were separated by sodium dodecyl sulphate-polyacrylamide gel electrophoresis, transferred to a polyvinylidene difluoride membrane, and then, blocked with 5% skim milk for 2 h. The primary antibodies were diluted in a blocking solution as follows: β-actin: mouse antibody, 1:1000; t-Akt: rabbit antibody, 1:2000; p-Akt (Ser 473): rabbit antibody, 1:1000; FOXO1: rabbit antibody, 1:1000; G6PC: rabbit antibody, 1:2000; SOCS3: rabbit antibody, 1:1000; and Anti-p-FOXO1 (p-Ser256): rabbit antibody, 1:1000. Antibodies were purchased from Cell Signalling Technology (Danvers, MA, USA), Proteintech Group (Rosemont, IL, USA), and Abcam (Cambridge, UK). The membrane was incubated with the primary antibodies at 4°C overnight and washed thrice for 10 min each. Next, the membrane was incubated with the secondary antibody at 18-30°C for approximately 50 min and washed thrice for 10 min each. Bands were displayed with a gel imager and quantified using Image-J. Standardisation was performed against β-actin.

RT-qPCR

Total RNA was extracted using the RNAsimple Total RNA Kit (Tiangen Biotech, Beijing, China), and the concentrations were determined using the NanoDrop 2000 (Fisher Scientific, Hampton, NH, USA). Reverse transcription was performed using PrimeScript RT with gDNA Eraser (Takara, Kusatsu, Japan). PCR was carried out using the Applied Biosystems 7300 Real-Time PCR System (Fisher Scientific) with SYBR Premix Ex Taq II (Takara) as follows: 3 min at 95°C and 41 cycles of 30 sec at 95°C, 5 sec at 95°C, and 31 sec at 60°C. The melting curve was constructed over a temperature of 60-95°C. Gene expression levels were normalised to β-actin using the $2^{-\Delta\Delta Ct}$ method [13]. All primers used in this study are listed in **Table 1**.

High-throughput sequencing

Total RNA was extracted using the RNeasy mini kit (Qiagen, Hilden, Germany). The sequencing library was constructed using the TruSeq RNA Sample Preparation Kit (Illumina, San Diego, USA), according to the manufacturer's instructions. Ribo-Zero rRNA was used to remove ribosomal RNA from the total RNA. After purification, the mRNA was fragmented using divalent cations at 94°C for 8 min. Using the RNA fragment as a template, the first-strand cDNA was replicated using reverse transcriptase and random primers. Second-strand cDNA synthesis was then performed using DNA polymerase I and RNase H. cDNA fragments underwent a terminal repair process, adding a single "A" base and then, joining the linker sequences. The purified product was amplified by PCR to generate the final cDNA library. Purified libraries were verified for insert size, and molar concentrations were calculated by Qubit 2.0 (Life Technologies, Carlsbad, CA, USA) and by Agilent

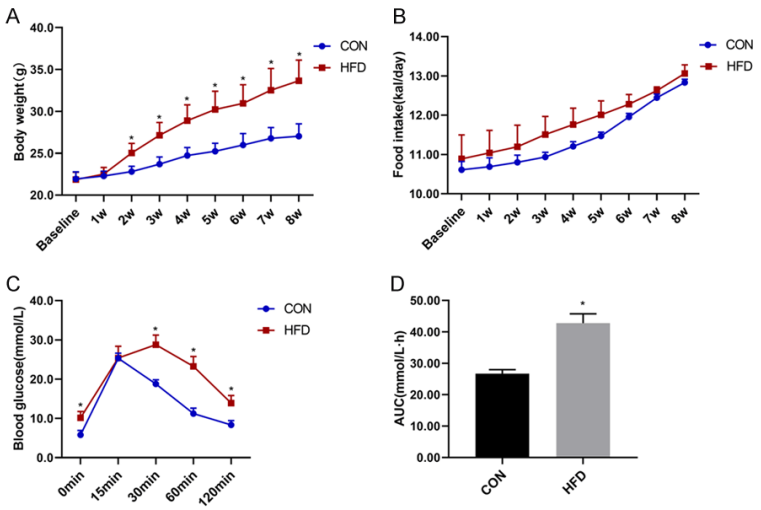

Figure 1. Body weights and food intake of C57BL/6J mice before and IPGTT experiment result after high-fat diet intervention for 8 weeks. A. Body weight in control and high-fat diet groups; B. Food intake in CON group and HFD group; C. Blood glucose levels at 0, 15, 30, 60, and 120 min following glucose intraperitoneal injection; D. The area under the curve for glucose levels. Data are presented as the mean ± SD (n=12 in CON and n=24 in HFD). Student's *t*-test was used for statistical analysis. **P* < 0.05 vs CON group.

2100 Bioanalyzer (Agilent Technologies, Santa Clara, CA, USA). Clusters were generated by cBot, diluted to a 10-pM library, and then, sequenced by the Illumina NovaSeq 6000. Library construction and sequencing were performed at Shanghai Sinomics (Shangai, China). High-throughput sequencing results have been uploaded to the GEO database. GEO accession number is GSE137840.

Identification and expression analysis of lncRNAs and mRNAs

lncRNA and mRNA were obtained from authoritative databases, lncRNA included RefSeq, Ensembls and Genebank, and mRNA included Noncode and Ensembls. Fragments in each gene segments were compared using StringTie [14] (Johns Hopkins University, Baltimore, MD, USA) and normalised with the trimmed mean of M values algorithm to calculate the Fragments Per Kilobase Million (FPKM) value of each gene. Differences in gene expressions were identified using the "edge" package in R based on the FPKM value. F-values were corrected by controlling the False Discovery Rate.

Establishment of cell model and analysis

Mouse liver cancer cells (Hepa) were purchased from the cell bank of the Chinese Academy of Sciences and stored at the Clinical Research Centre of Hebei General Hospital. Hepa cells were cultured in Dulbecco's Modified Eagle Medium (DMEM; Gibco) supplemented with 10% foetal bovine serum (Hyclone Laboratories, UT, USA), 1% non-essential amino acids (Gibco, Waltham, MA, USA), and 1% streptomycin (Hyclone Laboratories) and incubated in a 5% CO_2 atmosphere at 37°C. To establish the IR model, the cells were transferred to DMEM with 0.25 mmol L^{-1} palmitic acid (PA) upon reaching approximately 80% confluency [15]. Glucose concentration was determined using the Glucose Oxidase Assay kit (Applygen, Beijing, China) at 0 h, 8 h, 16 h, and 24 h after the transfer was used to validate the establishment of the cell IR model.

Hepa cells were cultured in 96-well plates and treated with 10 μM, 20 μM, 30 μM, 40 μM, or 50 μM RSV dissolved in DMSO (50 mmol L^{-1}) upon reaching approximately 80% confluency. Cell viability was calculated using CCK-8 (Dojindo, Kumamoto, Japan).

The cells were transfected in an incubator at 37°C upon reaching approximately 60% confluency. The transfection complex (200 μL OPTI-MEM, 5 μL RNA oligo stock solution, and 10 μL siRNA-Mate transfection reagent) was added to the medium at a final concentration of 50 nM siRNA. Hepa cells were divided into a control group and a knockdown group. RNA was extracted 24 h after transfection, and the knockdown efficiency of NONMMUT008655.2 was detected by RT-PCR. Hepa cells were seeded in 6-well plates, 24 h after transfection. PA and RSV were added to the corresponding groups, and cells were stimulated with insulin 24 h after treatment. Proteins were extracted for western blot 40 min after insulin stimulation.

Statistical analysis

All data were processed using SPSS 22.0 (IBM, Armonk, NY, USA), and the results were expressed as means ± standard deviation. One-

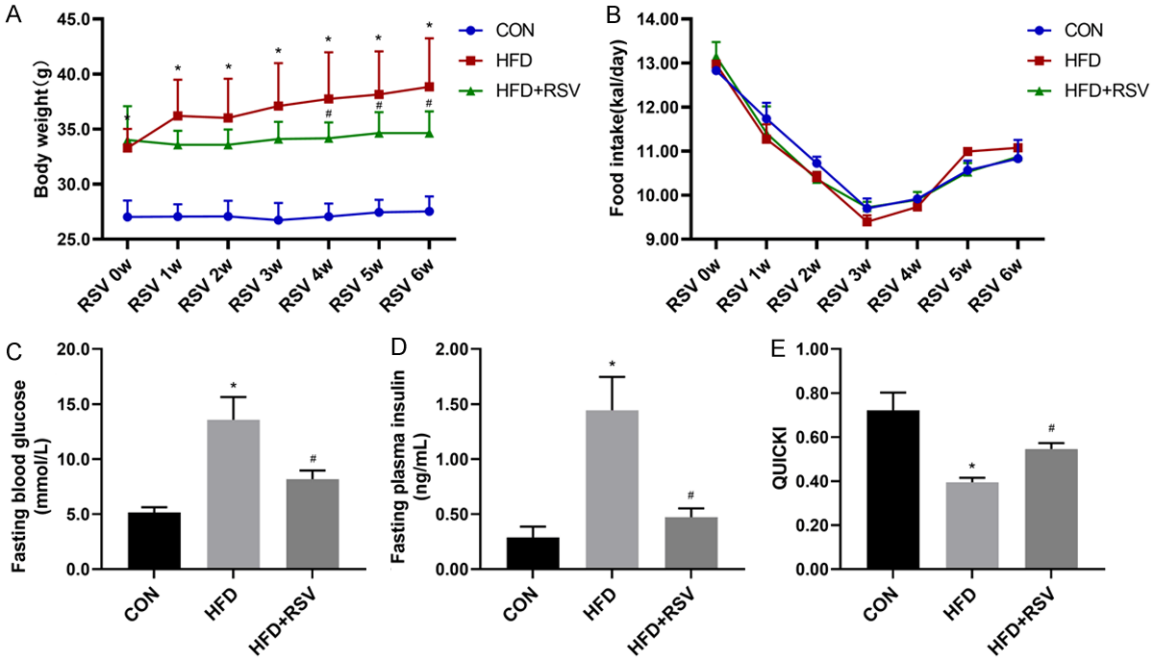

Figure 2. Body weight and insulin sensitivity indicators after resveratrol treatment. A. Body weights in control, high-fat diet and resveratrol-treated groups; B. Daily caloric intake in the three groups; C. Fasting blood glucose levels in the three groups; D. Fasting plasma insulin levels; E. Quantitative insulin sensitivity check index. Data are presented as the mean ± SD (n=12). One-way ANOVA was used for statistical analysis followed by a post hoc least significant difference test or Tamhane's multiple comparison test. **P* < 0.05 vs CON group. #*P* < 0.05 vs HFD group.

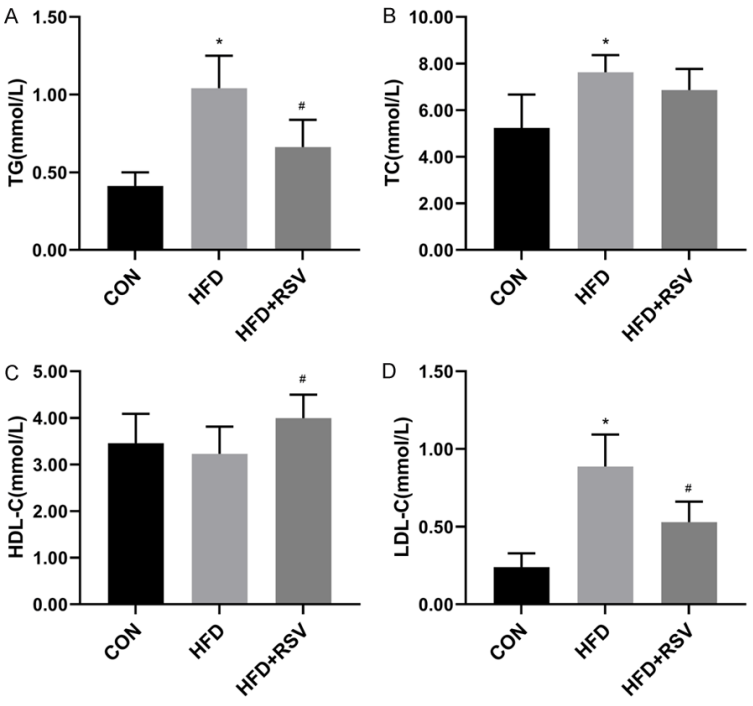

Figure 3. Lipid profiles after resveratrol treatment. A. Triglyceride; B. Total cholesterol; C. High-density lipoprotein cholesterol; D. Low-density lipoprotein cholesterol. Data are presented as the mean ± SD (n=12). One-way ANOVA was used for statistical analysis followed by a post hoc least significant difference test or Tamhane's multiple comparison test. **P* < 0.05 vs CON group. #*P* < 0.05 vs HFD group.

way analysis of variance (ANOVA) was used in conjunction with the Student's *t*-test to identify significant differences at $P < 0.05$. The differential expression of lncRNAs and mRNAs was expressed as *q-value* < 0.05, and the absolute value of fold-change was greater than or equal to a two-fold-change.

Results

Establishment of a high-fat diet-induced IR animal model

The baseline body weight of the control group (CON), and the high-fat diet group (HFD) did not differ significantly. However, after two weeks of diet intervention, the body weight of the HFD mice was significantly higher than that of CON (**Figure 1A**), although the mean daily caloric intake was similar between the two

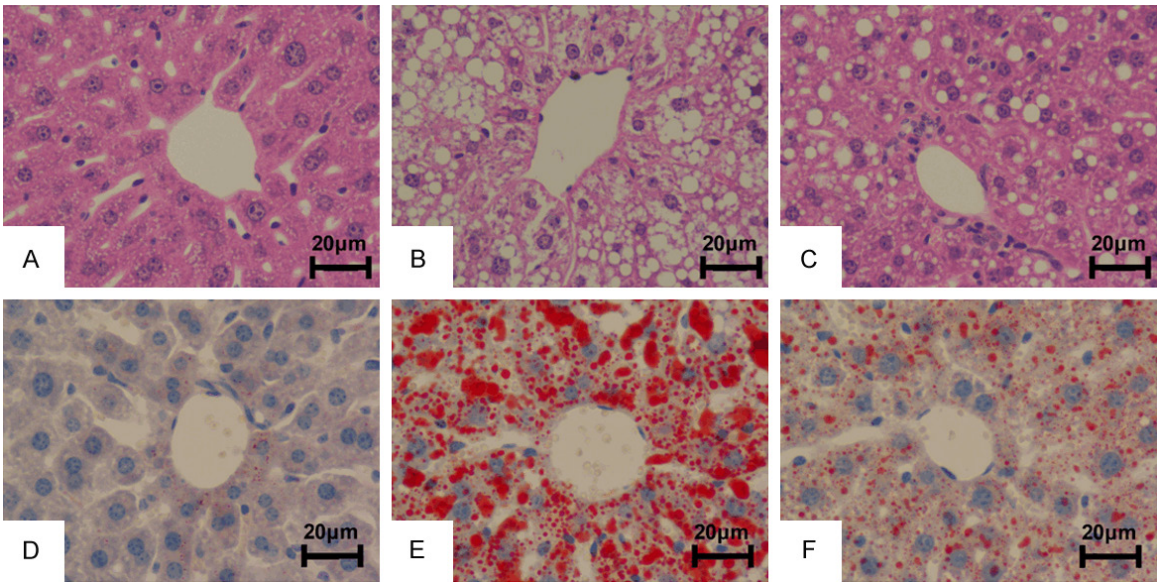

Figure 4. Hepatic lipid deposition after resveratrol treatment. A-C. H&E staining of liver tissue after resveratrol treatment; D-F. Oil Red O staining of liver tissue after resveratrol treatment; A, D. CON group had normal liver morphology; B, E. The HFD group had a large number of lipid droplet vacuoles; C, F. HFD+RSV group had fewer vacuoles compared with HFD alone. One-way ANOVA was used for statistical analysis followed by a post hoc least significant difference test. $^{*}P < 0.05$ vs CON group. $^{\#}P < 0.05$ vs HFD group.

groups (**Figure 1B**). Further, the intraperitoneal glucose tolerance test (IPGTT) after eight weeks of diet intervention showed that the blood glucose levels of HFD were significantly higher than those of the CON at 0 min, 30 min, 60 min, and 120 min after the glucose saline injection (**Figure 1C**). Additionally, the AUC for the HFD group was significantly higher than that of CON (**Figure 1D**), indicating that the IR model was established successfully.

General indices and blood lipid levels

The body weight of HFD mice was significantly higher than that of CON throughout the eight weeks of diet intervention, and compared to the HFD mice treated with RSV (HFD+RSV) after four weeks of diet intervention (**Figure 2A**), although the daily caloric intake did not differ significantly among the groups (**Figure 2B**). Further, the fasting blood glucose and insulin levels were significantly higher in HFD mice compared with those in CON and HFD+RSV (**Figure 2C**, **2D**); while the quantitative insulin sensitivity check index (QUICKI) of HFD mice was significantly lower than that of CON and HFD+RSV (**Figure 2E**).

The triglycerides (TG), TC, and low-density lipoprotein cholesterol (LDL-C) levels were significantly higher in HFD mice compared to those in the CON group. Moreover, RSV treatment significantly reduced TG and LDL-C, and increased HDL-C, however, was not observed to have an effect on TC (**Figure 3A-D**).

Liver lipid deposition

In the CON mice, the cellular structure of liver tissue was clear and intact, the cytoplasm was uniformly red-stained, and the lipid droplets were less vacuolated. Alternatively, in HFD mice, the cell structure of the liver tissue was disordered, and lipid droplets were irregularly sized in the cytoplasm. In the HFD+RSV group, the lipid droplets displaced the nucleus to the cell edge, the morphology of the liver tissue and the number of lipid droplets was intermediate to that of the CON and HFD groups (**Figure 4A-C**). Tissue from the CON group contained blue nuclei with a small number of orange-red lipid droplets, whereas numerous orange-red lipid droplets was observed in HFD (**Figure 4D-F**).

Expression profiles of lncRNAs and mRNAs

The expression of lncRNAs and mRNAs in CON, HFD, and HFD+RSV was determined using high-throughput sequencing. After standardisation,

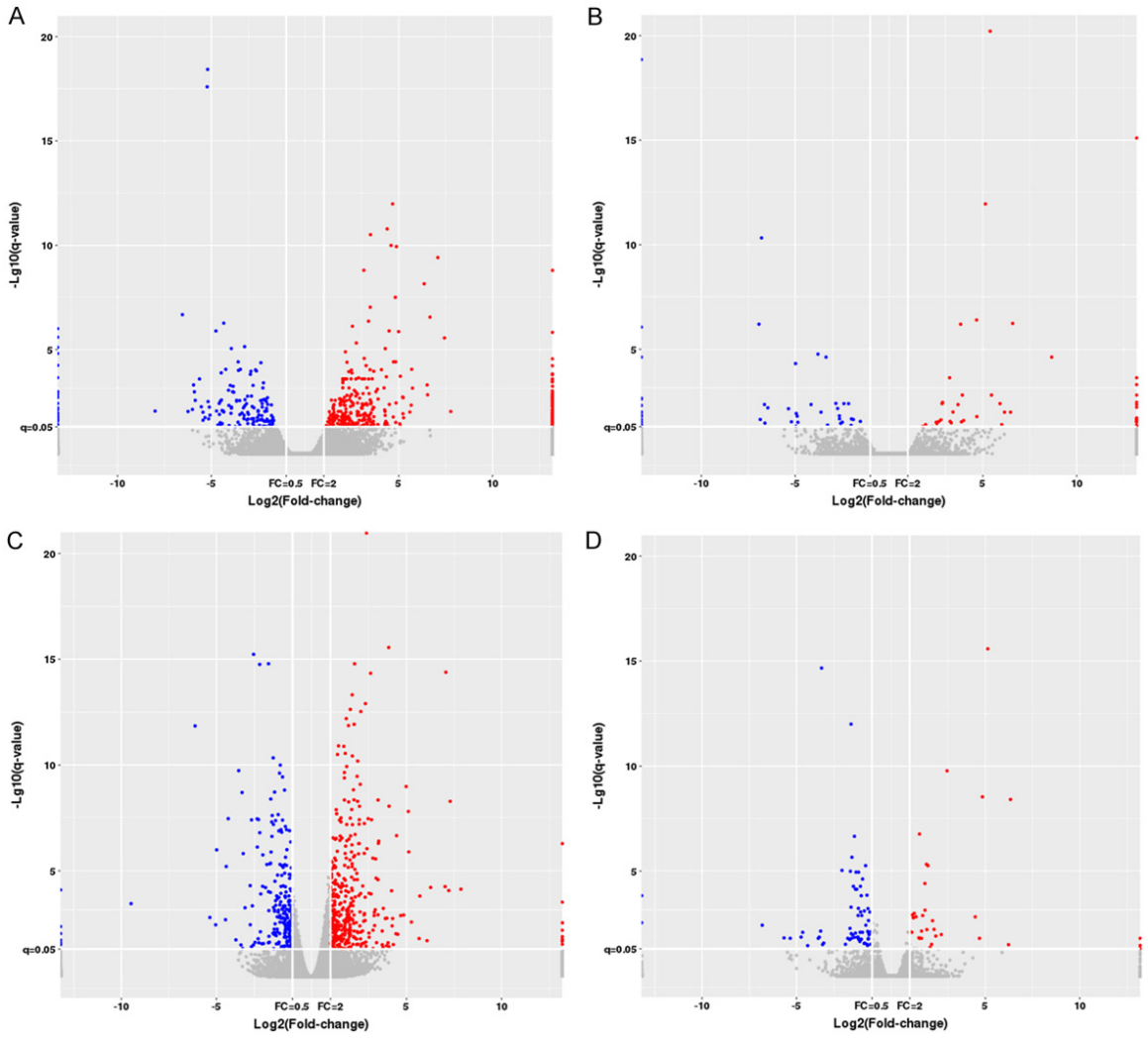

Figure 5. Volcano plot of lncRNA and mRNA variation between groups. A and B. lncRNAs; C and D. mRNAs; A and C. HFD vs CON; B and D. HFD+RSV vs HFD. Red area contains lncRNAs (or mRNAs) with $P < 0.05$ and fold-change ≥ 2. Blue area contains lncRNAs (or mRNAs) with $P < 0.05$ and fold-change ≤ -2.

a total of 51,024 lncRNAs and 31,055 mRNAs were detected in mouse liver tissues. Compared with CON, 503 differentially expressed lncRNAs (344 upregulated and 159 downregulated) and 655 differentially expressed mRNAs (418 upregulated and 237 downregulated) were detected in HFD. Compared with HFD, 95 differentially expressed lncRNAs (46 upregulated and 49 downregulated) and 102 differentially expressed mRNAs (34 upregulated and 68 downregulated) were detected in HFD+RSV (**Figure 5A-D**).

Of the lncRNAs and mRNAs upregulated in HFD, 25 lncRNAs and 50 mRNAs were downregulated in HFD+RSV. Of the lncRNAs and mRNAs downregulated in HFD, 25 lncRNAs and 23 mRNAs were upregulated in HFD+RSV. The expression patterns of lncRNAs and mRNAs were consistent within each group, however, differed significantly between the CON, HFD, and HFD+RSV groups (**Figure 6A** and **6B**; **Tables 2** and **3**).

Gene ontology (GO) and kyoto encyclopaedia of genes and genomes (KEGG) analysis

GO analysis classified differentially expressed mRNAs into three categories: biological process (BP), molecular function (MF), and cellular component (CC). The differential expression of mRNAs primarily included negative signal regulation, negative molecular function regulation, enzyme-linked receptor protein signalling path-

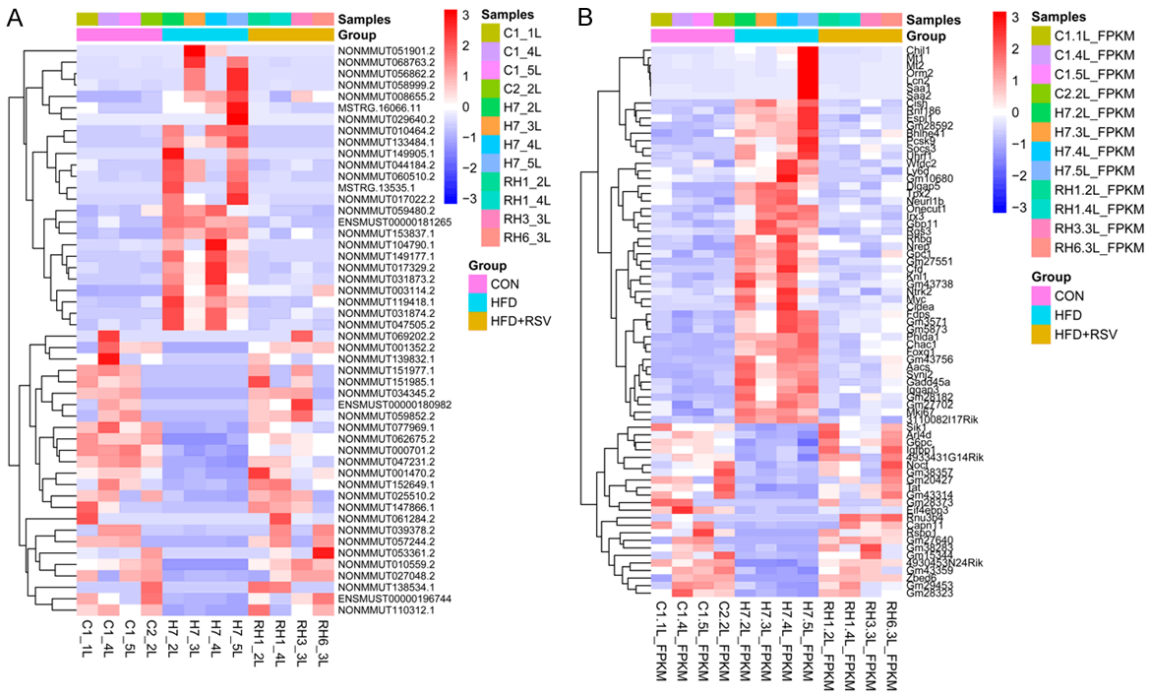

Figure 6. Clustering heat map of differentially expressed lncRNAs and mRNAs. A. lncRNAs; B. mRNAs. Red area contains lncRNAs (or mRNAs) with $P < 0.05$ and fold-change ≥ 2. Blue area contains lncRNAs (or mRNAs) with $P < 0.05$ and fold-change ≤ -2.

Table 2. Expression patterns of lncRNAs in mice fed a regular diet (CON), a high-fat diet (HFD), or an HFD and treated with resveratrol (HFD+RSV)

Seq name	Log2 (Fold-change)	Regulation (HFD vs CON)	Log2 (Fold-change)	Regulation (HFD+RSV vs HFD)
NONMMUT056862.2	6.53438	Up	-6.63876	Down
NONMMUT060510.2	5.23091	Up	-5.35853	Down
NONMMUT031873.2	4.87425	Up	-3.78681	Down
NONMMUT051901.2	4.85021	Up	-4.94198	Down
NONMMUT149177.1	4.81429	Up	-3.35448	Down
NONMMUT031874.2	4.38032	Up	-2.83355	Down
ENSMUST00000181265	3.66591	Up	-4.15283	Down
NONMMUT153837.1	3.49033	Up	-1.90271	Down
NONMMUT058999.2	3.38641	Up	-3.27548	Down
NONMMUT003114.2	3.13425	Up	-1.20431	Down
NONMMUT119418.1	3.15295	Up	-2.57853	Down
NONMMUT068763.2	3.10618	Up	-3.62327	Down
MSTRG.16066.11	2.79283	Up	-2.73949	Down
NONMMUT008655.2	2.73349	Up	-1.49769	Down
NONMMUT047505.2	2.55273	Up	-2.64522	Down
NONMMUT059480.2	2.34636	Up	-2.63681	Down
NONMMUT044184.2	1.93205	Up	-2.01973	Down
NONMMUT017329.2	1.60991	Up	-1.52653	Down
ENSMUST00000180982	-7.99741	Down	8.66425	Up
NONMMUT034345.2	-6.54169	Down	6.58842	Up
NONMMUT069202.2	-6.24163	Down	6.00385	Up

NONMMUT053361.2	-5.44591	Down	6.47468	Up
NONMMUT147866.1	-5.44114	Down	5.91095	Up
NONMMUT010559.2	-5.19587	Down	5.39012	Up
NONMMUT039378.2	-4.57962	Down	4.67744	Up
NONMMUT059852.2	-4.46208	Down	5.13582	Up
NONMMUT077969.1	-4.33904	Down	3.31442	Up
NONMMUT062675.2	-4.23117	Down	3.67421	Up
NONMMUT027048.2	-3.95038	Down	3.85579	Up
NONMMUT001352.2	-3.86435	Down	3.81448	Up
NONMMUT057244.2	-3.80355	Down	3.90188	Up
NONMMUT000701.2	-3.56772	Down	2.65998	Up
NONMMUT001470.2	-2.88807	Down	3.22941	Up
NONMMUT025510.2	-2.72927	Down	2.76835	Up
NONMMUT110312.1	-2.64181	Down	2.51996	Up
NONMMUT152649.1	-2.50569	Down	2.82238	Up
NONMMUT047231.2	-2.35594	Down	1.80211	Up
ENSMUST00000196744	-2.07075	Down	1.94977	Up

The table lists only some of the results for lncRNAs with an up- or downregulation in expression in the HFD group compared with the CON group and in the HFD+RSV group compared with the HFD group. Seq name, lncRNA name; fold-change, absolute fold-change between the compared groups.

Table 3. Top upregulated and downregulated mRNAs in mice fed a regular diet (CON), a high-fat diet (HFD), or an HFD and treated with resveratrol (HFD+RSV)

Gene name	Log2 (Fold-change)	Regulation (HFD vs CON)	Log2 (Fold-change)	Regulation (HFD+RSV vs HFD)
Saa2	7.86092	Up	-6.81613	Down
Cidea	7.29545	Up	-3.84703	Down
Saa1	7.21934	Up	-5.66038	Down
Gm43756	7.06443	Up	-2.16895	Down
Lcn2	7.02521	Up	-5.33297	Down
Cfd	6.96657	Up	-3.67247	Down
Orm2	5.70148	Up	-4.75652	Down
Chil1	5.25805	Up	-4.40776	Down
Gm27551	5.11722	Up	-2.28461	Down
Mt2	4.24141	Up	-4.66979	Down
Chac1	3.58132	Up	-1.73976	Down
Aacs	3.57367	Up	-1.81265	Down
Foxq1	3.56353	Up	-1.60571	Down
Iqgap3	3.53768	Up	-1.71281	Down
Dlgap5	3.49875	Up	-2.18024	Down
Socs3	2.42581	Up	-1.77296	Down
Gm43738	2.41071	Up	-1.73832	Down
Bhlhe41	2.29883	Up	-1.54587	Down
Gm3571	2.23722	Up	-1.32981	Down
Irx3	2.23361	Up	-2.10145	Down
Zbed6	-6.12237	Down	6.35215	Up
Gm28373	-5.34677	Down	4.68876	Up
Gm27640	-4.52201	Down	5.12685	Up
Capn11	-4.48551	Down	4.46449	Up
Gm20427	-3.22439	Down	2.66816	Up

Rnu3b4	-2.9713	Down	6.33207	Up
Eif4ebp3	-2.72848	Down	1.18786	Up
Gm43314	-2.07988	Down	1.96045	Up
Gm28323	-2.06383	Down	1.79928	Up
Gm38283	-1.96239	Down	2.37695	Up
Gm38357	-1.92091	Down	1.90174	Up
Gm29453	-1.82934	Down	1.51896	Up
Igfbp1	-1.78184	Down	2.20251	Up
Gm15344	-1.73828	Down	1.67884	Up
4933431G14Rik	-1.72561	Down	2.15402	Up
4930453N24Rik	-1.68061	Down	1.51409	Up
Noct	-1.40321	Down	1.62225	Up
Tat	-1.31374	Down	1.14191	Up
Gm43359	-1.29315	Down	1.02345	Up
Sik1	-1.14932	Down	1.23115	Up

The table lists only the top 20 of the results for mRNAs with an up- or downregulation in expression in the HFD group compared with the CON group and in the HFD+RSV group compared with the HFD group. Gene name, mRNA name; fold-change, absolute fold-change between the compared groups.

Figure 7. GO and pathway analysis of differentially-expressed mRNAs. A. Gene ontology analysis of differentially-expressed mRNAs; B. KEGG pathway analysis of differentially-expressed mRNAs.

way, enzyme inhibitor activity, and endopeptidase activity (**Figure 7A**). KEGG analysis further classified differentially expressed mRNAs into metabolic pathways, the mitogen-activated protein kinase signalling pathway, Janus kinase/signal transducers and activators of transcription (JAK/STAT) signalling pathway, insulin signalling pathway, as well as the cell cycle and adipocytokine signalling pathway (**Figure 7B**). The insulin signalling pathway was selected, and the closely related target gene mRNA *SOCS3* was detected.

Verification of lncRNAs

Four lncRNAs upregulated in HFD and downregulated in HFD+RSV (NONMMUT031874.2, NONMMUT003114.2, NONMMUT008655.2, and NONMMUT017329.2) along with three lncRNAs downregulated in HFD and upregulated in

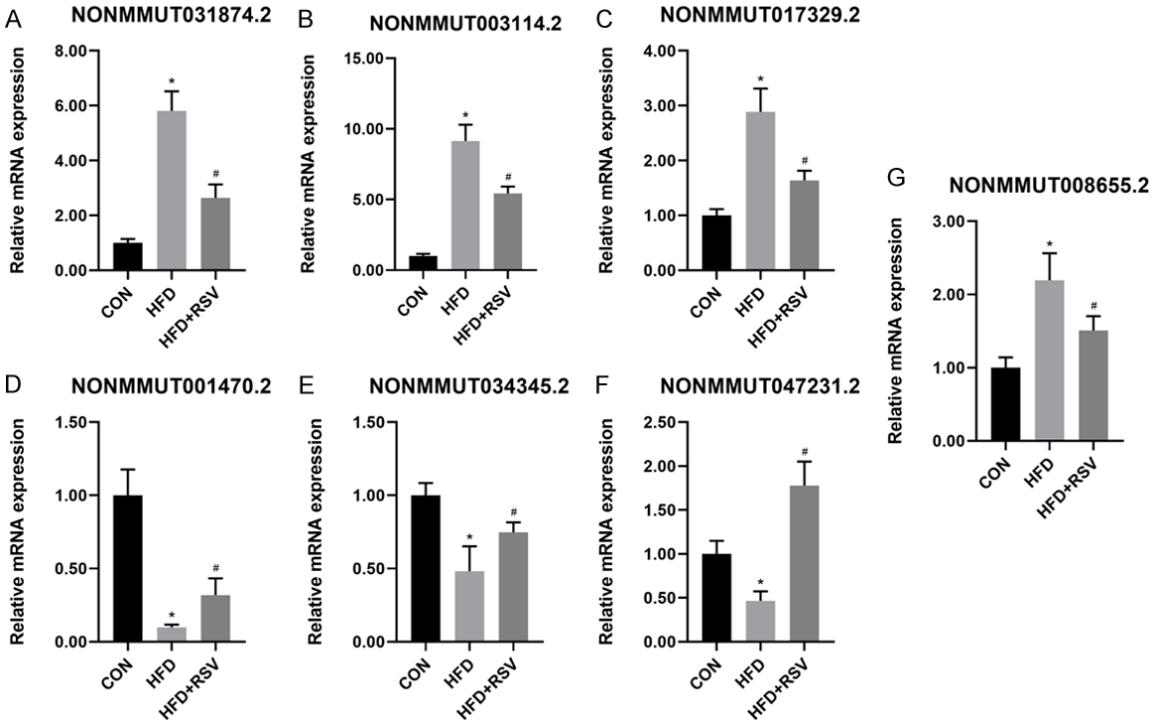

Figure 8. Validation of four HFD-upregulated and RSV-downregulated lncRNAs by RT-qPCR. A. NONMMUT031874.2; B. NONMMUT003114.2; C. NONMMUT017329.2; G. NONMMUT008655.2. Validation results of three HFD-downregulated and RSV-upregulated lncRNAs by RT-qPCR. D. NONMMUT001470.2; E. NONMMUT034345.2; F. NONMMUT047231.2. All results were obtained from three independent experiments. Data are presented as the mean ± SD (n=4). One-way ANOVA was used for statistical analysis followed by a post hoc least significant difference test or Tamhane's multiple comparison test. $^{*}P < 0.05$ vs CON, $^{\#}P < 0.05$ vs HFD.

HFD+RSV (NONMMUT034345.2, NONMMUT001470.2, and NONMMUT047231.2) were selected for real-time quantitative polymerase chain reaction (RT-qPCR) to verify sequencing results. The expression levels of the selected lncRNAs were consistent with those of the sequencing analysis (**Figure 8A-G**).

mRNA levels of insulin signalling pathway-related genes

No differences were identified in the mRNA level of *Akt* among CON, HFD, and HFD+RSV (**Figure 9A**). However, the mRNA levels of Forkhead Box O (FOXO1), Suppressor of Cytokine Signalling 3 (SOCS3), and Glucose-6-Phosphatase Catalytic Subunit (G6PC) were significantly higher in HFD compared to the CON group, and significantly lower in HFD+RSV compared to HFD (**Figure 9B-D**).

Protein expression related to insulin signalling pathway

Compared with CON, the expression levels of FOXO1, SOCS3, and G6PC were significantly increased in HFD, however, significantly decreased in HFD+RSV. Alternatively, no significant differences were identified in the expression levels of Akt among the three groups. The phosphorylation levels of FOXO1 and Akt were decreased in HFD compared with CON, and increased in HFD+RSV compared with HFD (**Figure 10A-G**).

NONMMUT008655.2 lncRNA-miRNA-mRNA co-expression network

From the seven selected lncRNAs, NONMMUT008655.2 exhibited the highest FPKM value (120.2). Path analysis and prediction revealed that the mRNA SOCS3 was related to NONMMUT008655.2, presenting a consistent trend. To clarify the interaction between SOCS3 and NONMMUT008655.2, we constructed a map of the lncRNA-miRNA-mRNA network and found that NONMMUT008655.2 regulates SOCS3 via miRNA mmu-miR-133c, mmu-miR-3569-5p, mmu-miR-504-3p, and mmu-miR-7076-5p. It was further revealed that both SOCS3 and NONMMUT008655.2 may play a key role in improving IR (**Figure 11**).

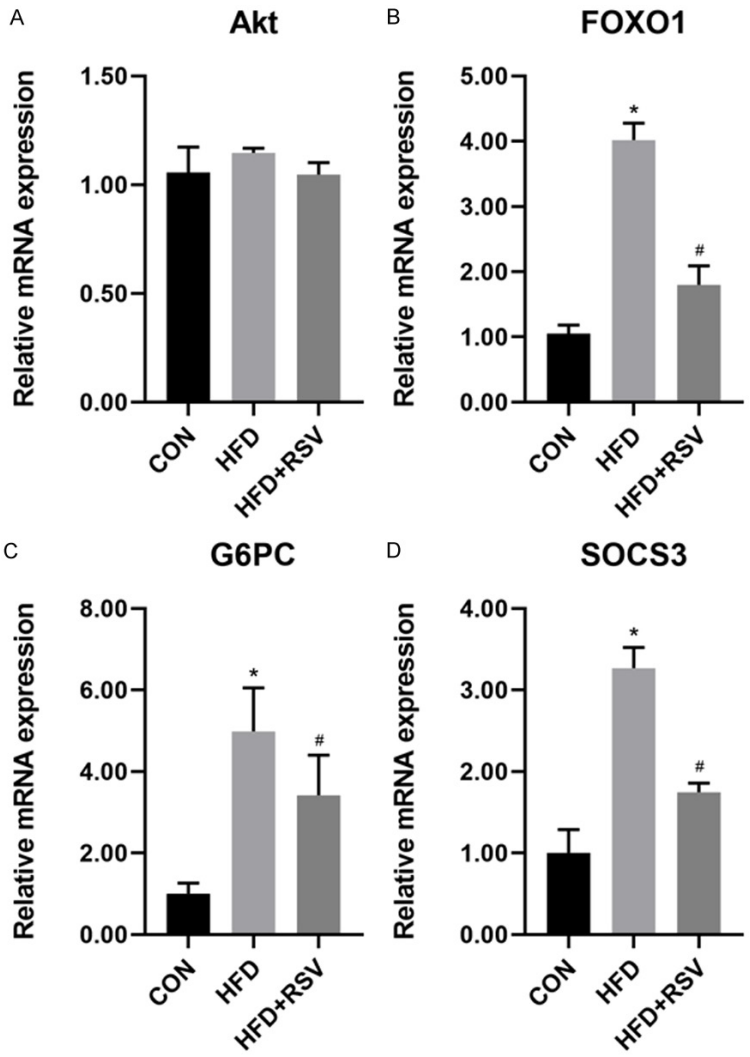

Figure 9. Relative mRNA expression of insulin signal pathway indicators in liver. A. Akt; B. FOXO1; C. G6PC; D. SOCS3. Data are presented as the mean ± SD (n=4). One-way ANOVA was used for statistical analysis followed by a post hoc least significant difference test or Tamhane's multiple comparison test. $^{*}P < 0.05$ vs CON, $^{\#}P < 0.05$ vs HFD.

Establishment of cell model

Glucose concentration was measured at 0 h, 8 h, 16 h, and 24 h after the transfer of cells to medium with or without PA and CON, respectively). At 0 h, 8 h, and 16 h, no significant differences were identified in glucose concentration between CON and PA. However, the glucose concentration in PA was significantly higher than that in CON at 24 h after transfer, indicating that the IR model was established successfully (**Figure 12A**) [16]. The glucose concentrations in the 0 h, 8 h, 16 h, and 24 h media of Hepa cells were impacted by both PA and RSV. Although, no significant difference in glucose concentration was observed in the medium between the three groups at 0 and 8 hours, by 16 and 24 hours, the glucose concentration in the PA group was significantly higher than that in the CON group. Moreover, at 24 hours, the glucose concentration in the RSV group was significantly lower than that in the HFD group, indicating that RSV effectively reduces the glucose concentration and improves IR (**Figure 12B**).

Cell viability

Cell viability was monitored after the treatment of Hepa cells with 0-50 μM RSV for 24 h. The results showed that 10 μM, 20 μM, and 30 μM RSV did not significantly affect the viability of Hepa cells (**Figure 12C**). Besides, the cell survival rate in PA (80.6%) was lower than that in the CON (87.1%), or PA+30 μM RSV (84.6%), however, the differences were not statistically significant (**Figure 12D**).

Effect of RSV on insulin signalling pathway after knockdown of NONMMUT008655.2

After the successful knockdown of NONMMUT008655.2 (**Figure 12E**), compared with CON, the expression of FOXO1, G6PC, and SOCS3 was significantly higher in PA, however the expression of p-Akt and p-FOXO1 was significantly lower. Moreover, the knockdown of NONMMUT008655.2 significantly increased the expression of p-Akt and p-FOXO1 compared with that in PA, yet significantly decreased the expression of FOXO1, G6PC, and SOCS3. The expression of FOXO1, G6PC, and SOCS3 was significantly lower in PA+RSV than in PA, whereas the expression of p-Akt and p-FOXO1 was significantly higher. Compared with the knockdown of NONMMUT008655.2, PA+RSV significantly increased expression of p-Akt and p-FOXO1, however, significantly decreased the expression of FOXO1 (**Figure 13A-G**).

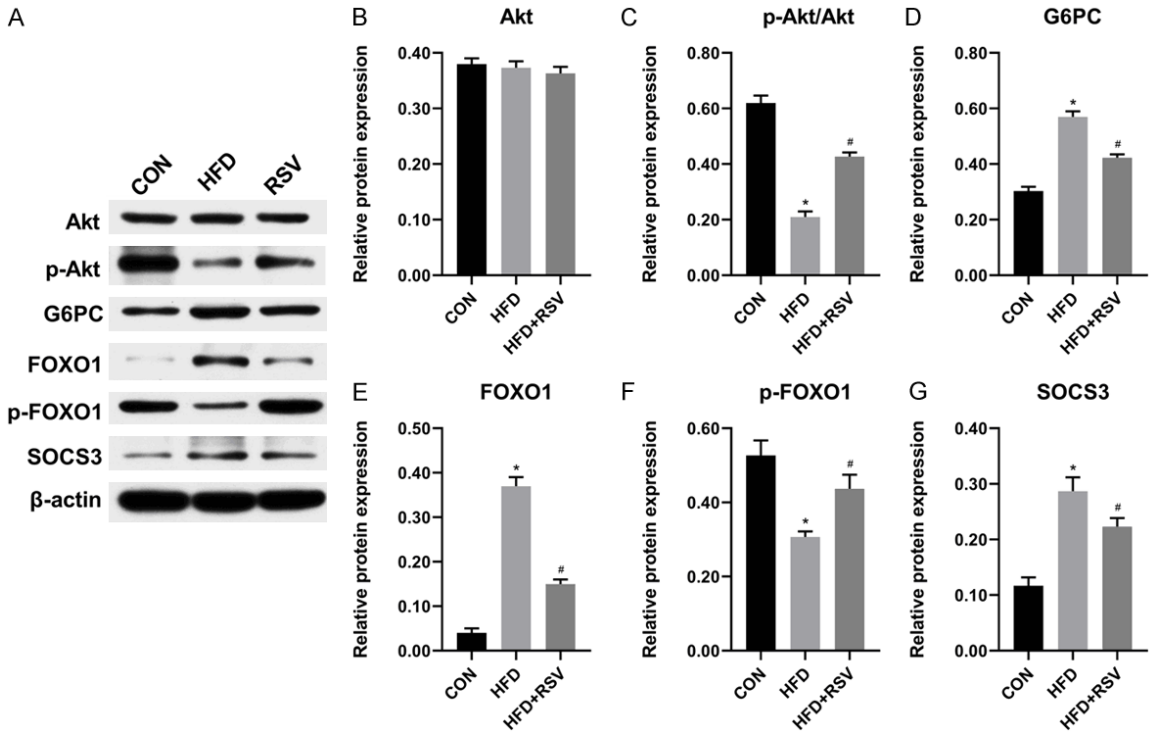

Figure 10. Relative protein expression of insulin signalling pathway indicators in liver. (A) Protein bands of insulin signal pathway molecules; (B) Akt; (C) p-Akt/Akt; (D) G6PC; (E) FOXO1; (F) p-FOXO1 and (G) SOCS3. Densitometric analysis of protein expression. Data are presented as the mean ± SD (n=3). One-way ANOVA was used for statistical analysis followed by a post hoc least significant difference test or Tamhane's multiple comparison test. $^{*}P < 0.05$ vs CON, $^{\#}P < 0.05$ vs HFD.

Discussion

In addition to its anti-tumour, anti-inflammatory, antioxidant, anti-ageing, cardioprotective, and neuroprotective properties, RSV has also been reported to improve IR [17, 18]. The pathogenesis of T2DM is complex as the target organs of insulin include the skeletal muscle, liver, and fat cells [19]. It has been reported that RSV reduces blood sugar, improves IR in T2DM, and protects the function of islet beta cells by activating the insulin signalling pathway thereby allowing insulin to bind insulin receptors on the cell membrane and activate the insulin receptor substrate protein [20]. The liver is an insulin-sensitive organ, and an important site for glycolipid metabolism. Previous studies on the HFD-induced T2DM animal model has shown that RSV effectively reduces hepatocyte IR and hepatic steatosis, and improves abnormalities in glycolipid metabolism by activating the SIRT1 and AMPK signalling pathways in hepatocytes, while inhibiting inflammatory signalling pathways [7, 21].

In the present study, RSV not only reduced the blood glucose, insulin index, and AUC in HFD mice, but also improved QUICKI, blood lipid levels, and the histomorphology of hepatocytes. These results indicate that mice fed a HFD experience inhibition of the insulin signalling pathway, and RSV improves IR while reducing hepatic lipid deposition, TG, and LDL-C, however, does not significantly impact TC or HDL-C. The effect of RSV on different blood lipid indicators is related to the subject type, drug concentration, administration route, experimental duration, and test tissue [22].

Although lncRNAs were originally considered to be transcriptional gene "noise", numerous studies have since indicated that they regulate gene expression and participate in a variety of important biological processes, including chromatin modification, transcription and post-transcriptional regulation, cell proliferation, differentiation, and apoptosis. Besides, lncRNAs are closely associated with the development of human diseases, including T2DM, cardiovascu-

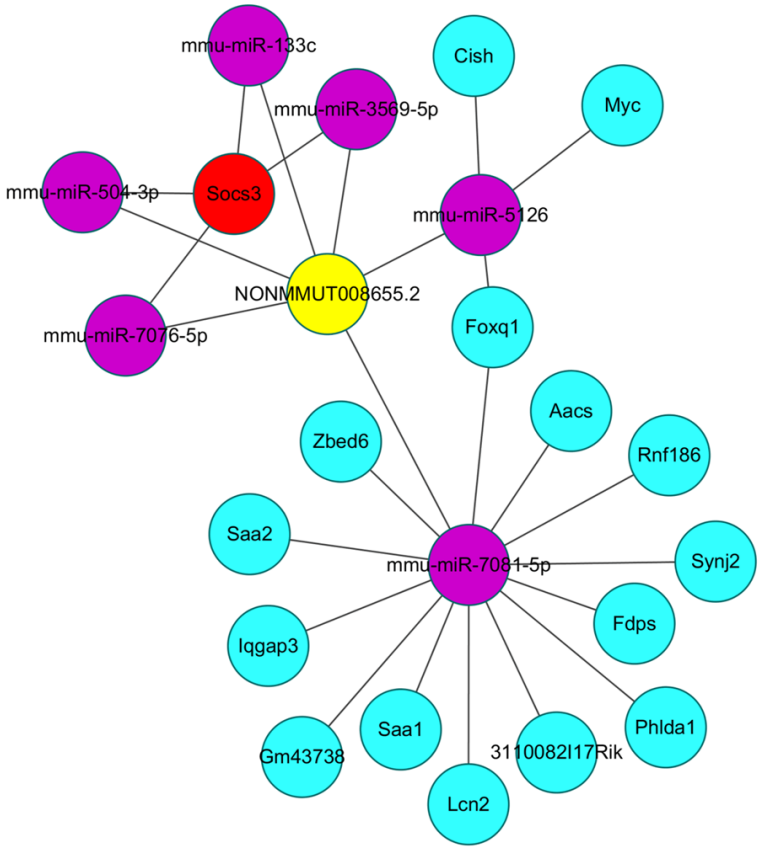

Figure 11. The NONMMUT008655.2 lncRNA-miRNA-mRNA network. This co-expression network suggests an inter-regulation of lncRNAs, miRNA and mRNAs.

lar, blood, neurodegenerative, and lung diseases, as well as various cancers [23-27]. To our knowledge, this is the first study to report on the modulation of lncRNAs in the insulin signalling pathway of an HFD-induced insulin-resistant mouse model administrated RSV.

High-throughput sequencing revealed 503 differentially expressed lncRNAs in HFD mice compared with the CON group and a further 95 differentially expressed lncRNAs compared with the HFD+RSV group. Moreover, the expression of 50 lncRNAs in the HFD+RSV group was opposite to that in HFD; of these, 25 upregulated lncRNAs in HFD were downregulated in HFD+RSV. Many of these lncRNAs are intergenic regions that may regulate the expression of genes encoding adjacent proteins [28]. RT-qPCR verified the sequencing results, indicating that RSV improves HFD-induced IR by regulating the expression of lncRNAs in the mouse liver. However, the role of these lncRNAs in increasing insulin sensitivity remains unclear. Additionally, the expression of 50 lncRNAs was reversed by RSV within the HFD group. Moreover, GO and KEGG analysis classified these lncRNAs as part of the insulin signalling pathway and indicated that NONMMUT008655.2 exhibited the highest expression. The lncRNA-miRNA-mRNA network map revealed that NONMMUT008655.2 regulates *SOCS3* through mmu-miR-133c, mmu-miR-3569-5p, mmu-miR-504-3p, and mmu-miR-7076-5p [29]. SOCS3 is an important suppressor of cytokine signalling that regulates JAK/STAT, and is likely related to IR [30]. Akt regulates a variety of signalling pathways, including those associated with cell survival, metabolism, differentiation, and proliferation. Akt is also a key molecule in the insulin signalling pathway as it regulates glycogen synthesis and glucose transport in the liver. Phosphorylated Akt inhibits FOXO1 expression and activates that of phosphorylated FOXO1, which transfers FOXO1 from the nucleus to the cytoplasm, inhibiting its transcriptional activity [31]. In the liver, FOXO1 promotes G6PC expression, which is the rate-limiting enzyme of the gluconeogenesis pathway, thereby increasing hepatic glucose production and, consequently, blood sugar. Inhibition of FOXO1 downregulates G6PC, decreases blood glucose, and improves IR [32]. Previous studies have reported that overexpression of SOCS3 inhibits the phosphorylation and activation of Akt, as well as the phosphorylation of JAK2 and STAT3, which in turn inhibits Akt activation, indicating an important link between Akt and SOCS3 [33].

NONMMUT008655.2 is expressed in mouse hepatocytes and is considered to be associated with RSV to improve IR. In the present study, Hepa cells were used to establish an *in vitro* IR model to explore the relationship between RSV and NONMMUT008655.2 [16]. Our results indicate that administration of 30 μM RSV for 24 h

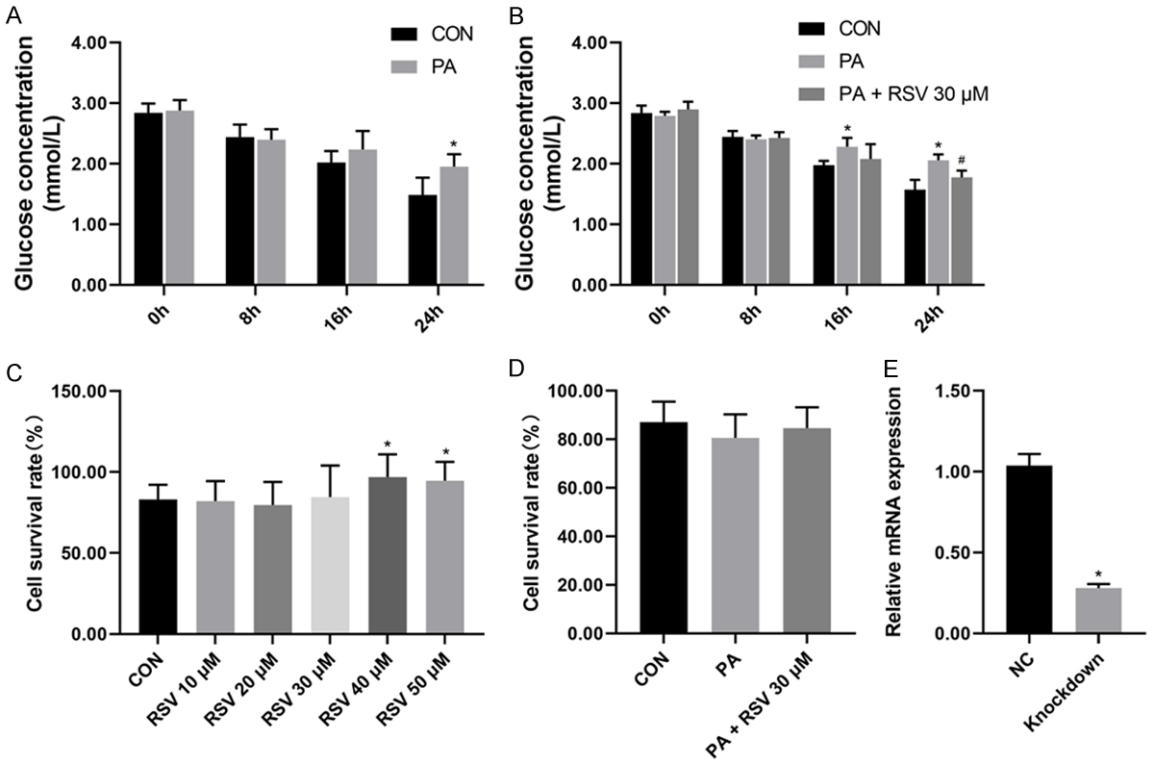

Figure 12. Establishment of an insulin-resistant cell model and transfection efficiency after NONMMUT008655.2 knockdown. A. Glucose concentration in the culture medium after PA treatment for 0, 8, 16, and 24 hours; B. Glucose concentrations in Hepa cells after PA and RSV treatments; C. Cell survival rate after 24 hours of treatment with different concentrations of resveratrol; D. Cell survival rates of the different groups after PA and resveratrol treatments; E. Relative mRNA level of NONMMUT008655.2. Data are presented as the mean ± SD (n=8). One-way ANOVA was used for statistical analysis followed by a post hoc least significant difference test or Tamhane's multiple comparison test.*$P < 0.05$ vs CON, #$P < 0.05$ vs HFD.

reduced the glucose concentration of PA-treated Hepa cells and improved IR [34].

Previous studies showed that lncRNAs play an important role in improving IR as a key regulator of gene expression in the insulin signalling pathway [35]. It has been suggested that lncRNAs affect the development of T2DM by regulating the development of islet beta cells and insulin secretion [36]; however, the role of NONMMUT008655.2 remained unclear. In the present study, we verified the associated molecules in the Akt-FOXO1 pathway by RT-qPCR and western blot and identified the potential regulatory role of RSV and NONMMUT008655.2. After knocking down NONMMUT008655.2, we analysed changes in the insulin signalling pathways and observed an improvement in IR *in vitro*. Compared with knockdown NONMMUT008655.2, RSV improved IR more effectively via regulating the expression of p-Akt, p-FOXO1, and FOXO1; however, no significant changes in the expression were observed for G6PC and SOCS3. These results indicate that the pharmacological effects of RSV are similar to the downregulation of NONMMUT008655. Similarly, RSV improves HFD-induced IR by downregulating NONMMUT008655.2 *in vivo*.

In summary, high-throughput sequencing revealed that RSV may improve hepatic IR by downregulating NONMMUT008655.2. Additionally, the lncRNA and the encoded protein showed similar expression patterns, suggesting that the lncRNA may regulate the interaction of the encoded transcript and protein in the insulin signalling pathway. Finally, our data suggests that NONMMUT008655.2 miRNA mmu-miR-133c, mmu-miR-3569-5p, mmu-miR-504-3p, mmu-miR-7076-5p and mRNA SOCS3 could represent novel pathways for T2DM treatment using RSV.

Conclusions

Our data suggests that RSV improves hepatic IR and controls blood sugar levels by downregu-

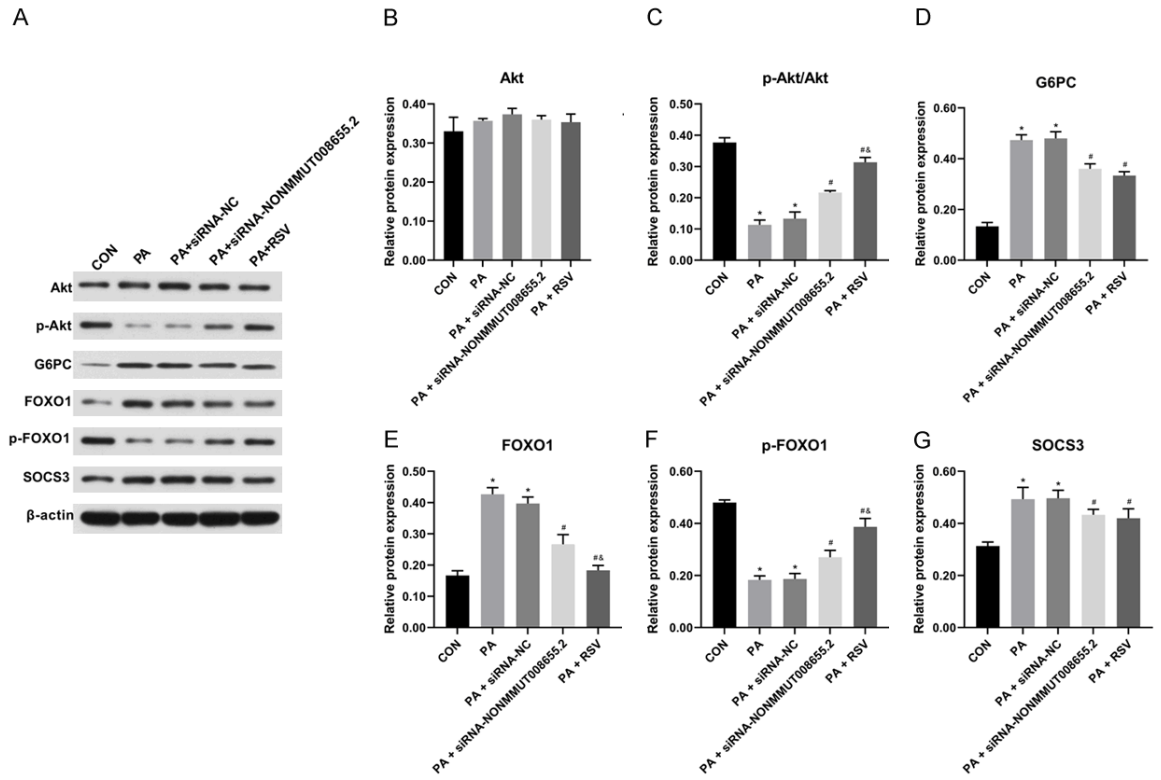

Figure 13. Effect of resveratrol on the insulin signalling pathway after knockdown of NONMMUT008655.2. A. Protein bands of insulin signalling pathway molecules; B. Akt; C. p-Akt/Akt; D. G6PC; E. FOXO1; F. p-FOXO1; G. SOCS3. Data are presented as the mean ± SD (n=3). One-way ANOVA was used for statistical analysis followed by a post hoc least significant difference test or Tamhane's multiple comparison test. $^{*}P < 0.05$ vs CON, $^{\#}P < 0.05$ vs PA, $^{\&}P < 0.05$ vs PA + siRNA-NONMMUT008655.2.

lating NONMMUT008655.2. Hence, RSV and NONMMUT008655.2 may serve as potential therapeutic targets for IR and T2DM.

Acknowledgements

We sincerely thank the teachers at the Clinical Medical Research Centre of Hebei General Hospital who helped us during the experiment. We thank Ning Li for responding to reviewers' and editor's comments. This study was supported by the grant from the Natural Science Foundation of Hebei Province (No. H201830-7071).

Disclosure of conflict of interest

None.

Abbreviations

RSV, Resveratrol; LncRNA, Long-chain non-coding RNA; HFD, High-fat diet; SOCS3, Suppressor of cytokine signalling 3; SOCS3, Suppressor of cytokine signalling 3; G6PC, Glucose-6-phosphatase catalytic subunit; FOXO1, Forkhead box O1; Akt, Protein kinase B; T2DM, Type-2 diabetes mellitus; IR, Insulin resistance; IPGTT, Intraperitoneal glucose tolerance test; AUC, Area under the curve; QUICKI, Quantitative insulin sensitivity check index; TG, Triglycerides; TC, Total cholesterol; HDL-L, High-density lipoprotein cholesterol; LDL-L, Low-density lipoprotein cholesterol; mRNA, Messenger RNA; BP, Biological process; BP, Biological process; MF, Molecular function; CC, Cellular component; JAK, Janus kinase; STAT, Signal transducers and activators of transcription; miRNA, microRNA; PA, Palmitic acid; SIRT1, Silent mating type information regulation 2 homolog-1; AMPK, AMP-activated protein kinase.

Address correspondence to: Guangyao Song, Department of Endocrinology, Hebei General Hospital, 348, Heping West Road, Shijiazhuang 050051, Hebei, People's Republic of China. Tel: +86-311-85988556; E-mail: guangyaosong123@163.com

References

[1] Ning G. Decade in review-type 2 diabetes mellitus: at the centre of things. Nat Rev Endocrinol 2015; 11: 636-638.

[2] Guariguata L, Whiting DR, Hambleton I, Beagley J, Linnenkamp U and Shaw JE. Global estimates of diabetes prevalence for 2013 and projections for 2035. Diabetes Res Clin Pract 2014; 103: 137-149.

[3] Akash MSH, Rehman K and Liaqat A. Tumor necrosis factor-alpha: role in development of insulin resistance and pathogenesis of type 2 diabetes mellitus. J Cell Biochem 2018; 119: 105-110.

[4] Rehman K, Akash MSH, Liaqat A, Kamal S, Qadir MI and Rasul A. Role of interleukin-6 in development of insulin resistance and type 2 diabetes mellitus. Crit Rev Eukaryot Gene Expr 2017; 27: 229-236.

[5] Biasutto L, Mattarei A, Azzolini M, La Spina M, Sassi N, Romio M, Paradisi C and Zoratti M. Resveratrol derivatives as a pharmacological tool. Ann N Y Acad Sci 2017; 1403: 27-37.

[6] Thiel G and Rossler OG. Resveratrol regulates gene transcription via activation of stimulus-responsive transcription factors. Pharmacol Res 2017; 117: 166-176.

[7] Zhao H, Chen S, Gao K, Zhou Z, Wang C, Shen Z, Guo Y, Li Z, Wan Z, Liu C and Mei X. Resveratrol protects against spinal cord injury by activating autophagy and inhibiting apoptosis mediated by the SIRT1/AMPK signaling pathway. Neuroscience 2017; 348: 241-251.

[8] Jiang Z, Chen K, Cheng L, Yan B, Qian W, Cao J, Li J, Wu E, Ma Q and Yang W. Resveratrol and cancer treatment: updates. Ann N Y Acad Sci 2017; 1403: 59-69.

[9] Ravasi T, Suzuki H, Pang KC, Katayama S, Furuno M, Okunishi R, Fukuda S, Ru K, Frith MC, Gongora MM, Grimmond SM, Hume DA, Hayashizaki Y and Mattick JS. Experimental validation of the regulated expression of large numbers of non-coding RNAs from the mouse genome. Genome Res 2006; 16: 11-19.

[10] Liu XF, Hao JL, Xie T, Pant OP, Lu CB, Lu CW and Zhou DD. The BRAF activated non-coding RNA: a pivotal long non-coding RNA in human malignancies. Cell Prolif 2018; 51: e12449.

[11] Weidle UH, Birzele F, Kollmorgen G and Rüger R. Long non-coding RNAs and their role in metastasis. Cancer Genom Proteom 2017; 14: 143-160.

[12] Bhatt JK, Thomas S and Nanjan MJ. Resveratrol supplementation improves glycemic control in type 2 diabetes mellitus. Nutr Res 2012; 32: 537-541.

[13] Livak KJ and Schmittgen TD. Analysis of relative gene expression data using real-time quantitative PCR and the 2(-delta C(T)) method. Methods 2001; 25: 402-408.

[14] Buchfink B, Xie C and Huson DH. Fast and sensitive protein alignment using DIAMOND. Nat Methods 2015; 12: 59-60.

[15] Zhang H, Ge Z, Tang S, Meng R, Bi Y and Zhu D. Erythropoietin ameliorates PA-induced insulin resistance through the IRS/AKT/FOXO1 and GSK-3β signaling pathway, and inhibits the inflammatory response in HepG2 cells. Mol Med Rep 2017; 16: 2295-2301.

[16] Yanuka-Kashles O, Cohen H, Trus M, Aran A, Benvenisty N and Reshef L. Transcriptional regulation of the phosphoenolpyruvate carboxykinase gene by cooperation between hepatic nuclear factors. Mol Cell Biol 1994; 14: 7124-7133.

[17] Abbasi Oshaghi E, Goodarzi MT, Higgins V and Adeli K. Role of resveratrol in the management of insulin resistance and related conditions: mechanism of action. Crit Rev Clin Lab Sci 2017; 54: 267-293.

[18] Zhu X, Wu C, Qiu S, Yuan X and Li L. Effects of resveratrol on glucose control and insulin sensitivity in subjects with type 2 diabetes: systematic review and meta-analysis. Nutr Metab (Lond) 2017; 14: 60.

[19] Szkudelski T and Szkudelska K. Resveratrol and diabetes: from animal to human studies. Biochim Biophys Acta 2015; 1852: 1145-1154.

[20] Kim J, Bilder D and Neufeld TP. Mechanical stress regulates insulin sensitivity through integrin-dependent control of insulin receptor localization. Genes Dev 2018; 32: 156-164.

[21] Sung MM, Kim TT, Denou E, Soltys CM, Hamza SM, Byrne NJ, Masson G, Park H, Wishart DS, Madsen KL, Schertzer JD and Dyck JR. Improved glucose homeostasis in obese mice treated with resveratrol is associated with alterations in the gut microbiome. Diabetes 2017; 66: 418-425.

[22] Haghighatdoost F and Hariri M. Effect of resveratrol on lipid profile: an updated systematic review and meta-analysis on randomized clinical trials. Pharmacol Res 2018; 129: 141-150.

[23] Wang X, Chang X, Zhang P, Fan L, Zhou T and Sun K. Aberrant expression of long non-coding RNAs in newly diagnosed type 2 diabetes indicates potential roles in chronic inflammation and insulin resistance. Cell Physiol Biochem 2017; 43: 2367-2378.

[24] Freedman JE and Miano JM. National Heart, Lung, and Blood Institute workshop participants*; challenges and opportunities in linking long noncoding RNAs to cardiovascular, lung, and blood diseases. Arterioscler Thromb Vasc Biol 2017; 37: 21-25.

[25] Quan Z, Zheng D and Qing H. Regulatory roles of long non-coding RNAs in the central nervous

system and associated neurodegenerative diseases. Front Cell Neurosci 2017; 11: 175.
[26] Liu Y, Li Y, Xu Q, Yao W, Wu Q, Yuan J, Yan W, Xu T, Ji X and Ni C. Long non-coding RNA-ATB promotes EMT during silica-induced pulmonary fibrosis by competitively binding miR-200c. Biochim Biophys Acta 2018; 1864: 420-431.
[27] Yang G, Lu X and Yuan L. LncRNA: a link between RNA and cancer. Biochim Biophys Acta 2014; 1839: 1097-1109.
[28] Zare Javid A, Hormoznejad R, Yousefimanesh HA, Zakerkish M, Haghighi-Zadeh MH, Dehghan P and Ravanbakhsh M. The impact of resveratrol supplementation on blood glucose, insulin, insulin resistance, triglyceride, and periodontal markers in type 2 diabetic patients with chronic periodontitis. Phytother Res 2017; 31: 108-114.
[29] Zahra Z, Faezeh F, Mohammad ER, Alireza K and Ali M. Curcumin exerts beneficial role on insulin resistance through modulation of SOCS3 and Rac-1 pathways in type 2 diabetic rats. J Funct Foods 2019; 60.
[30] Pedroso JA, Buonfiglio DC, Cardinali LI, Furigo IC, Ramos-Lobo AM, Tirapegui J, Elias CF and Donato J Jr. Inactivation of SOCS3 in leptin receptor-expressing cells protects mice from diet-induced insulin resistance but does not prevent obesity. Mol Metab 2014; 3: 608-618.
[31] Zhou X, Zeng XY, Wang H, Li S, Jo E, Xue CC, Tan M, Molero JC and Ye JM. Hepatic FoxO1 acetylation is involved in oleanolic acid-induced memory of glycemic control: novel findings from Study 2. PLoS One 2014; 9: e107231.
[32] Lin X, Shi H, Cui Y, Wang X, Zhang J, Yu W and Wei M. Dendrobium mixture regulates hepatic gluconeogenesis in diabetic rats via the phosphoinositide-3-kinase/protein kinase B signaling pathway. Exp Ther Med 2018; 16: 204-212.
[33] Wu K, Chang Q, Lu Y, Qiu P, Chen B, Thakur C, Sun J, Li L, Kowluru A and Chen F. Gefitinib resistance resulted from STAT3-mediated Akt activation in lung cancer cells. Oncotarget 2013; 4: 2430-2438.
[34] Jin H, Zhang H, Ma T, Lan H, Feng S, Zhu H and Ji Y. Resveratrol protects murine chondrogenic ATDC5 cells against LPS-induced inflammatory injury through up-regulating MiR-146b. Cell Physiol Biochem 2018; 47: 972-980.
[35] Yan C, Chen J and Chen N. Long noncoding RNA MALAT1 promotes hepatic steatosis and insulin resistance by increasing nuclear SREBP-1c protein stability. Sci Rep 2016; 6: 22640.
[36] Akerman I, Tu Z, Beucher A, Rolando DMY, Sauty-Colace C, Benazra M, Nakic N, Yang J, Wang H, Pasquali L, Moran I, Garcia-Hurtado J, Castro N, Gonzalez-Franco R, Stewart AF, Bonner C, Piemonti L, Berney T, Groop L, Kerr-Conte J, Pattou F, Argmann C, Schadt E, Ravassard P and Ferrer J. Human pancreatic β cell lncRNAs control cell-specific regulatory networks. Cell Metab 2017; 25: 400-411.